Applied Geochemistry 103 (2019) 23–30

Contents lists available at ScienceDirect

Applied Geochemistry

journal homepage: www.elsevier.com/locate/apgeochem

Aluminum hydroxide coatings in limestone drains

Sheyla B. Palomino-Ore[a], J. Donald Rimstidt[a], John A. Chermak[a], Madeline E. Schreiber[a,*], Robert R. Seal II[b]

[a] Department of Geosciences, 926 W. Campus Drive, Virginia Tech, Blacksburg, VA, 24061, United States
[b] U.S. Geological Survey, 954 National Center, Reston, VA, 20192, United States

ARTICLE INFO

Editorial handling by Kate Marie Campbell

Keywords:
Limestone drain
Acid mine drainage
Acidity

ABSTRACT

This paper describes a mixed flow reactor experiment and associated data analysis scheme that are well suited for studying the chemical and physical processes that occur in limestone drains used to treat acid mine drainage (AMD). The experiment simulates the slowly evolving, near steady state, reactions that form coatings on limestone. The resulting coatings can be recovered for analysis of their structure and composition. Analysis of the time evolution of the composition of the effluent solutions is used to isolate and understand key factors that affect limestone drain performance.

The experiment investigated reactions between acidic aluminum sulfate solutions and calcite. The aluminum sulfate feed solutions contained 0.002–0.01 molal (32–329 mg/kg) Al and had pH values ranging from 3.7 to 4.2. At the beginning each experiment, the rate of H^+ consumption by reaction with the calcite was fast causing a distinct increase of the effluent pH. The pH increase caused some of the dissolved Al to precipitate as a coating on the calcite surfaces. The coating blocked the transfer of ions to and from the calcite causing the reaction rates to be limited by ion diffusion through the coating. The continued growth of the coating caused it to become an increasingly effective barrier to ion transport, which caused the neutralization rate to slow and the effluent solution pH to decline toward that of the feed solution. Powder X-ray diffraction (XRD) and scanning electron microscopy with energy dispersive spectroscopy (SEM-EDS) suggested that the coatings were mostly poorly crystalline gibbsite. Effluent solutions were analyzed to determine pH along with Al, Ca and S concentrations. The coating thickness at each sample time was estimated from the amount of Al lost from the solution since the beginning of the experiment. This thickness and the Ca and H^+ fluxes were used to find the apparent H^+ diffusion coefficient in the coatings.

1. Introduction

Acid mine drainage (AMD) is a widespread and persistent environmental problem that results from exposure of iron sulfides to air and water. Ideally this problem would be managed by isolating the iron sulfides from the atmosphere so that they could no longer interact with air and water but that approach is often physically or economically impractical. That means that some form of treatment of the AMD to reduce acidity and concentrations of toxic trace elements is the management practice of choice at most AMD sites. One of the most common treatments involves reaction of the AMD solutions with calcium carbonate through the use of limestone drains, which are channels filled with ~5- to 10 cm-sized pieces of limestone (Cravotta, 2008b; Cravotta et al., 2010; Cravotta and Trahan, 1999; Cravotta and Watzlaf, 2002; Skousen et al., 2017). Reaction of the AMD with limestone removes the primary acidity (H^+) from the AMD along with latent acidity (H^+ produced by the hydrolysis of dissolved Al and Fe) and increases the bicarbonate alkalinity, which is then available for further acid neutralization in receiving waters.

Limestone drains are easy to construct, use inexpensive and environmentally benign materials, and operate for extensive periods of time with only periodic maintenance. As AMD solutions flow through a limestone drain, H^+ is consumed by reaction with calcite in the limestone. At low pH (< ~6.3) the reaction produces carbonic acid and at higher pH (> 6.3) bicarbonate ions are produced, as respectively described by the equations:

$$CaCO_3(calcite) + 2\,H^+ = Ca^{2+} + H_2CO_3 \quad (1)$$

$$CaCO_3(calcite) + H^+ = Ca^{2+} + HCO_3^- \quad (2)$$

* Corresponding author.
E-mail addresses: sheylapalomino@gmail.com (S.B. Palomino-Ore), jdr02@vt.edu (J.D. Rimstidt), jchermak@vt.edu (J.A. Chermak), mschreib@vt.edu (M.E. Schreiber), rseal@usgs.gov (R.R. Seal).

https://doi.org/10.1016/j.apgeochem.2019.02.004
Received 19 July 2018; Received in revised form 11 January 2019; Accepted 5 February 2019
Available online 11 February 2019
0883-2927/

As these reactions remove H^+, the pH increases, which causes cations to hydrolyze and release more H^+ (latent acidity). Net acidity in AMD is the sum of the free H^+ concentration and the H^+ released from latent acidity produced by the hydrolysis of Fe^{2+}, Fe^{3+}, Mn^{2+}, and Al^{3+} (Kirby and Cravotta, 2005).

The most important of these reactions produce a variety of poorly crystalline to amorphous Fe and Al oxyhydroxides and hydroxysulfates such as ferrihydrite, schwertmannite, gibbsite, and basaluminite. These phases can incorporate or adsorb trace elements (e.g. As, Cd, Zn, Cu), removing them from the AMD and limiting their discharge into receiving waters. Unfortunately, some of the Fe and Al phases adhere to the limestone surfaces. These coatings then become a barrier to the transport of H^+ from the solution to the limestone surface, which slows the neutralization rate. In addition, they fill void spaces in the limestone bed, reducing its hydraulic conductivity. This gradual reduction in neutralization capacity and flow rate leads to the eventual failure of the installation.

Improving the performance of limestone drain requires knowledge gained from four sources. First, flow-through laboratory experiments, like the one described in Huminicki and Rimstidt (2008), are needed to understand the underlying chemistry and physics of the transport and neutralization processes. Second, larger scale tests (Cravotta, 2003; Cravotta et al., 2004) are needed to determine how well models developed from laboratory studies can scale to field conditions. Note that the laboratory-scale "cubitainer" test is an externally recycled batch reactor that produces concentration versus time data that must be differentiated twice in order to see the effect of coating growth. Third, monitoring of the behavior of installed drains (Cravotta, 2008b; Cravotta and Trahan, 1999; Cravotta et al., 2008; Hedin et al., 1994; Skousen and Ziemkiewicz, 2005; Watzlaf et al., 2000) is needed to determine whether their performance matches the predictions of the design models. Finally, failure analyses of defunct limestone drains (Robbins et al., 1999; Santomartino and Webb, 2007) can establish the reasons for declining performance.

Limestone drains are dynamic systems where the H^+ and cations that are removed by chemical reactions are constantly replenished by the flowing solution. This creates local steady state conditions rather than local equilibrium conditions (Rimstidt, 2015). This means that modeling limestone drain behavior requires a more sophisticated approach than provided by geochemical models that are based solely on the local equilibrium assumption (LEA). We need to understand how the reaction rates, diffusion rates, and flow rates are coupled in order to develop effective steady state models (Cravotta, 2008b). Some previous laboratory studies of limestone neutralization of acid waters containing Fe (Santoro et al., 1987) or Al (Volpicelli et al., 1981) did not consider the role of Fe and Al coatings and modeled the neutralization rate by assuming that it is controlled by diffusion through a static fluid layer adjacent to the solid surface. More recent studies indicated that reactions that produce coatings should be modeled by accounting for diffusion rates in the coatings (Huminicki and Rimstidt, 2008, 2009).

This paper describes a simple and flexible experiment that can be used to identify, isolate, and quantify the key factors that affect reactions between limestone, or other neutralization materials, and the chemical components of AMD under nearly steady state conditions. The custom-designed mixed flow reactor needed for the experiment can be manufactured quickly and at low cost using 3D printing technology (Michel et al., 2018). The reactor can accommodate a range of materials at different grain sizes. The resulting data can be analyzed to obtain quantitative information about the relationship between neutralization rates and coating development. Implementation of the experiment is illustrated by investigating the formation of Al coatings on calcite surfaces.

The Al precipitation reaction was chosen for this study because dissolved Al is toxic to organisms in receiving waters, is an important source of coatings found in limestone drains, and is a significant contributor to latent acidity in AMD solutions. The Al concentration range chosen for this study was based on concentrations that are typical of AMD (Fig. 1). At the low pH of AMD, Al is mobilized from aluminosilicate minerals in amounts that increase with decreasing pH. Low pH waters with elevated Al concentrations adversely impact the viability of aquatic organisms present in receiving waters (Camargo et al., 2009; Cravotta et al., 2010; Gensemer and Playle, 1999; Henry et al., 1999; Soucek et al., 2003; Teien et al., 2006). Aluminum toxicity to algae and fish is affected by pH and the concentrations of Ca, P, F, and dissolved organic matter (Gensemer and Playle, 1999). Using limestone drains to remove the dissolved Al mitigates this significant environmental impact of AMD. However, much of the Al accumulates in the limestone drains, slowly reducing their effectiveness until they fail. Several studies conducted to evaluate the effectiveness of limestone drain treatments have documented the formation of gypsum coatings (Huminicki and Rimstidt, 2008) and Fe-Al hydroxysulfate and oxyhydroxides (Hammarstrom et al., 2003; Soucek et al., 2003; Watzlaf et al., 2000).

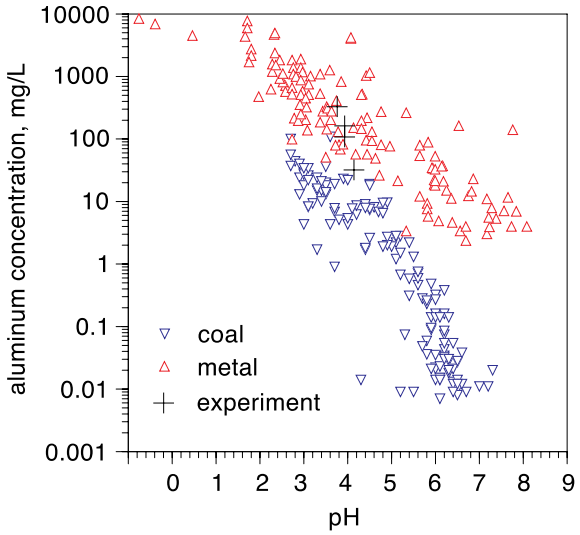

Fig. 1. Dissolved Al concentrations versus pH in acid mine drainage from coal mines (Cravotta, 2008a), metal mines (Plumlee et al., 1999) and for the initial conditions of the laboratory experiments described in this study.

2. Methods

A mixed flow reactor (MFR) experiment was used to study the reaction rates of aluminum sulfate solutions with calcite. The solution in a MFR is well mixed, so the effluent solution is a representative sample of the reactor contents. See Rimstidt (2014) for a detailed explanation of MFR performance. As a result, the effluent concentrations reflect the solution composition that produced the observed rate (Rimstidt and Dove, 1986). This allows the reaction rates to be measured directly, without the need to differentiate concentration versus time data as is generally done for batch reactors.

The reactor design is shown in Fig. 2. The reactor body was manufactured by 3D printing based on a design that was slightly modified from that published by Michel et al. (2018). This modified design has ledges on the wall near the bottom of the reactor that support a platform that holds the crushed calcite just above a magnetic stir bar. The feed solution was stored in a 2 L plastic tank and was introduced into the reactor using a peristaltic pump. The reactor was placed on a stir plate to keep the solution well-mixed. The effluent solution was collected in 15 mL glass tubes using a fraction collector.

The Iceland spar calcite crystals used for the experiments were free of visible inclusions. They were crushed and sieved (18–20 mesh) to recover the 850–1000 μm fractions, then rinsed briefly with DI. The specific geometric surface area was calculated to be 0.00214 m^2/g. The feed solution was made by dissolving 66.601 g of reagent grade

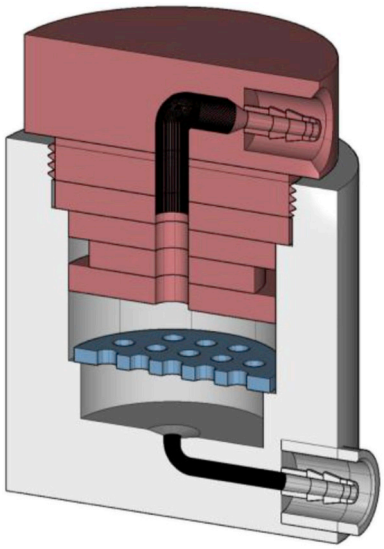

Fig. 2. Schematic diagram of the mixed flow reactor used in this study. Red = cap; blue = platform. The outside diameter of the body is 50 mm and the height is 50 mm. The diameter of the cap is 45 mm and height of the assembled reactor is 65 mm. The internal volume is ~7 cm^3. The feed solution enters at the bottom of the reactor and the effluent solution exits at the top. Solids are held on the platform. Stir bar sits below the platform. Illustration compliments of F. Marc Michel. (For interpretation of the references to color in this figure legend, the reader is referred to the Web version of this article.)

$Al_2(SO_4)_3$•$18H_2O$ in 1 kg deionized water to create a 0.1 molal stock solution. This solution was diluted to yield run solutions with Al concentrations of 0.01, 0.006, 0.004, and 0.001 molal (329, 162, 108 and 32 mg/kg, respectively). The experiments were named according to their starting Al concentration in mg/kg followed by the replicate number. For example, the first experiment using the 329 mg/kg Al solution would be 329–1.

Experiments were performed at room temperature of 25 ± 1 °C. At the beginning of each experiment 2.1 g of the crushed calcite was placed on the mesh and feed solution was pumped into the bottom of the reactor at a rate of approximately 0.02 g/sec. The experiment began (time = 0) when the reactor was completely filled so that the solution discharged from the top of the reactor. Effluent solution was collected into pre-weighed 15 mL tubes for 9 min intervals. The sample tubes were weighed before and after sample collection, and the mass of solution collected was divided by the collection time to calculate the flow rate. The pH was measured using an Ag/AgCl pH electrode calibrated with buffers at pH values of 7.00 and 4.00 for each measurement. The samples were preserved for chemical analysis by acidifying with nitric acid to pH less than 2. Each experiment ran for between 3 and 4 h. After each experiment, the calcite grains were recovered, dried, and stored in plastic tubes. The grains were not rinsed after reaction to avoid dislodging coatings.

The fluxes of dissolved species (J_i, mol/m^2sec) to or from the calcite is calculated from the difference between the concentrations in the feed and effluent solutions multiplied by the solution flow rate and divided by the total calcite surface area (see chapter 4 in Rimstidt, 2014), as described by the equation:

$$J_i = \frac{(m_i(\text{feed}) - m_i(\text{discharge}))r_{\text{flow}}}{A_{\text{calcite}}} \quad (3)$$

The total Al, Ca, and S concentrations in the feed and sample solutions were measured using inductively coupled plasma - optical emission spectroscopy (Spectro Arcos ICP-OES) at the Virginia Tech Soil and Plant Analysis Laboratory. The samples were not filtered and there was no visual evidence of precipitates in the solution before adding nitric acid. Sulfate was calculated from the S concentrations assuming that sulfate was the only S species in solution. Repeat measurements of selected samples showed averaged agreement between the samples of ± 1.47% for Al, ± 1.68% for Ca, and ± 0.91% for S (n = 4).

To obtain sufficient coating for X-ray diffraction (XRD) analysis, 0.5 × 0.5 × 0.1 cm cleavage pieces of Iceland spar calcite were immersed in 0.01, 0.004, and 0.002 molal aluminum sulfate solutions for 168 h in batch reactors. After the formation of a sufficient quantity of coating, the calcite pieces were recovered and dried. Coatings were removed by either lightly scraping the calcite surface or peeling them directly from the surface. XRD patterns of the coating materials were obtained using a Rigaku benchtop X-ray diffractometer with a diffracted beam monochromator for Cu Kα radiation with a scan range of 3–88° 2θ, a scan rate of 0.02° 2θ/min, and an accuracy better than 0.01°.

A Hitachi Tabletop Scanning Electron Microscope (TM3000) with energy dispersive spectral analysis was used to image the coatings from both MFR and batch experiments to conduct qualitative chemical mapping.

3. Results

Eight experiments were performed. For four experiments (329–1, 162–1, 108–1, and 32–1), the pH along with the Al, Ca, and S concentrations in selected effluent samples were determined and used for the subsequent calculations. Only the pH was determined for the other four experiments (329–2, 162–2, 108–2, and 32–2), which were performed under identical conditions to the first series of experiments to show that the neutralization patterns were essentially identical for replicate experiments. Fig. 3 shows the evolution of pH along with Al, Ca, and S concentration for four experiments. All data (Tables S1–S6) are provided in Supplementary Information.

Initially the Al concentrations in the effluent solutions (Fig. 3) were considerably lower than in the feed solutions because of its rapid precipitation onto the calcite surface. The Al concentrations in the effluent solution steadily increased and reached a nearly steady state value after 2 or 3 h. By the end of the experiment, the Al concentrations in the effluent solutions were between 80 and 93% of the influent concentration. As the coatings grew on calcite, they impeded the transport of H^+, produced by Al hydrolysis in the solution, to the calcite surface, thereby reducing the neutralization and Al hydrolysis rates. The growing Al hydroxide coating caused the neutralization reaction to slow because of the increasing diffusion path length between the solution and the calcite surface. The slowing neutralization rate allowed the effluent solution H^+concentrations to increase over time (i.e. the effluent pH decreased) as shown in Fig. 3. The reaction between calcite and H^+, equation (1), released Ca into solution so the effluent Ca concentrations were high at the beginning of the experiment, when the dissolution rates were fast, and decreased over time, as the neutralization rate declined. Sulfate concentrations in the effluent solutions were nearly constant (Fig. 3).

A second series of experiments (329–2, 169–2, 108–2 and 32–2) was used to test the reproducibility of the pH for replicate experiments. The average fractional difference between the measured pH at the same time points in these two sets of experiments was 0.49, 3.31, 6.32 and 2.46% respectively. Replicate measurements of Al, Ca and S for selected samples in the experiments were within ± 5.1% of each other.

In the batch experiments used to prepare coatings for XRD analysis, a white film appeared on the surface of calcite after ~1 h. After ~4 h, a distinct coating had formed (Fig. 4). This coating was collected and used for XRD analysis. XRD analysis of the coating material formed from a solution with an initial Al concentration of 270 mg/kg suggests that the coating consists primarily of poorly crystalline gibbsite (Fig. 5). Additional batch reactor experiments with initial Al concentrations of 54 mg/kg and 108 mg/kg also produced material showing peaks corresponding to poorly crystalline gibbsite.

Fig. 6 shows a back-scattered electron image, along with Al and S

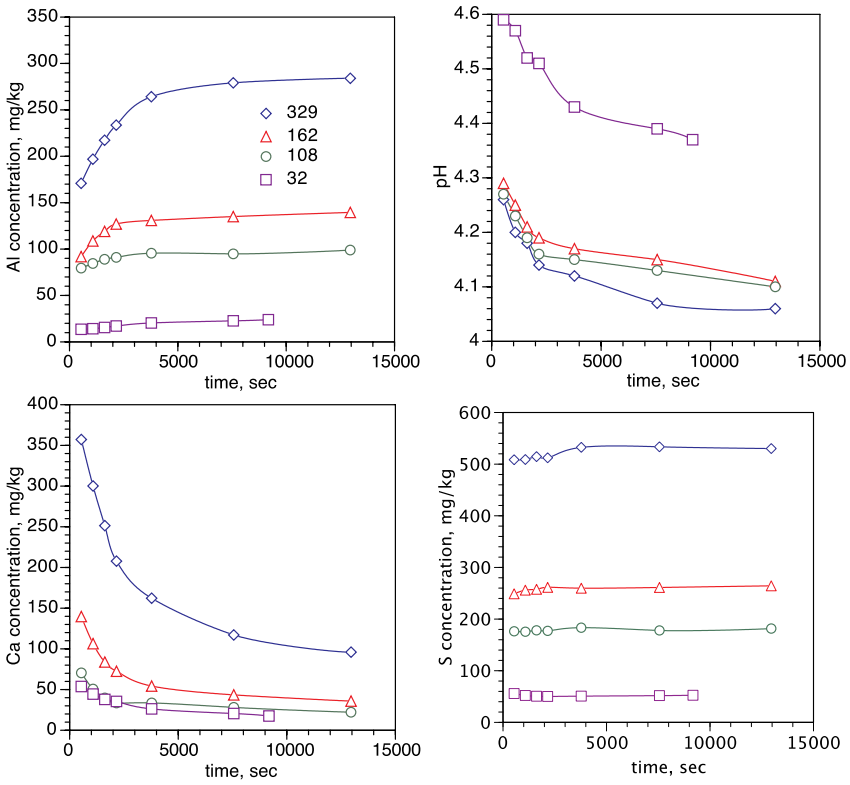

Fig. 3. Measured pH and concentrations of Al, Ca, and S in the effluent solutions over time for different feed solution Al concentrations (mg/kg) in the MFR experiments. The experiment number identifies the Al concentration (mg/kg) in the feed solution.

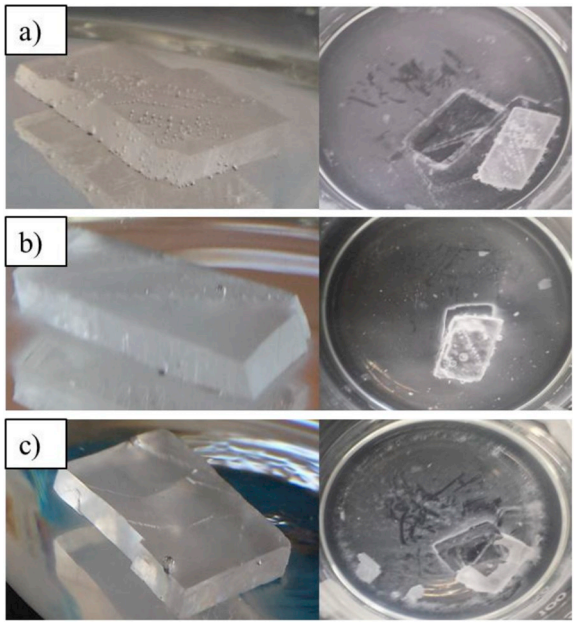

Fig. 4. Photographs of the coating that formed on the calcite from the batch experiments with Al concentrations of (a) 270 mg/kg, (b) 108 mg/kg, and (c) 54 mg/kg (diameter of petri dish is 9 cm). Left: After 4 h. Right: After 7 days (168 h).

chemical maps, for a coating formed in the MFR by reacting cleaved calcite with a solution containing 32 mg/kg Al for 4 h. These maps indicate that a very small amount of S is present in the coating (Fig. 6c), suggesting that basaluminite may have formed, although the mass percent of S is quite low (< 3%) in coating (Fig. 6d).

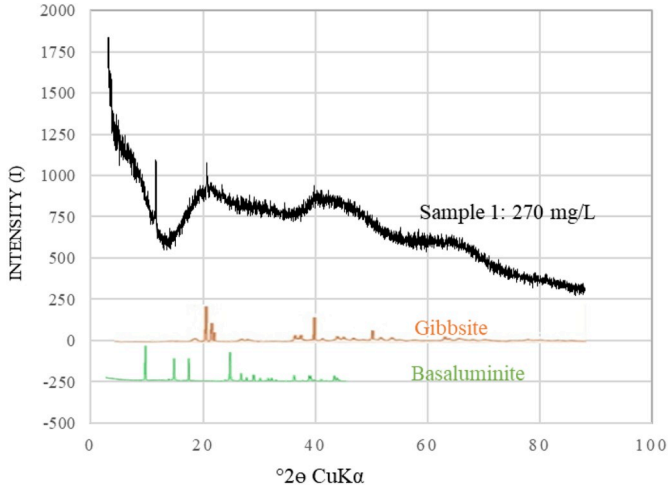

Fig. 5. Powder XRD pattern for a calcite coating formed by 7 day (168 h) reaction with a solution initially containing 270 mg/kg Al. The peak positions for well-crystallized gibbsite (orange) and basaluminite (green) are shown for comparison. (For interpretation of the references to color in this figure legend, the reader is referred to the Web version of this article.)

4. Discussion

The coatings in limestone drains typically consist of multiple, poorly crystalline phases that are difficult to identify and characterize. XRD patterns for the coatings recovered from our experiments (Fig. 5) suggest that the coatings consist of poorly crystalline gibbsite. This is consistent with the activity diagram shown in Fig. 7, which shows that the effluent solutions have compositions that plot in the gibbsite stability field, indicating that they are supersaturated with that phase. Gibbsite has been reported as a precipitate in AMD (Bigham and

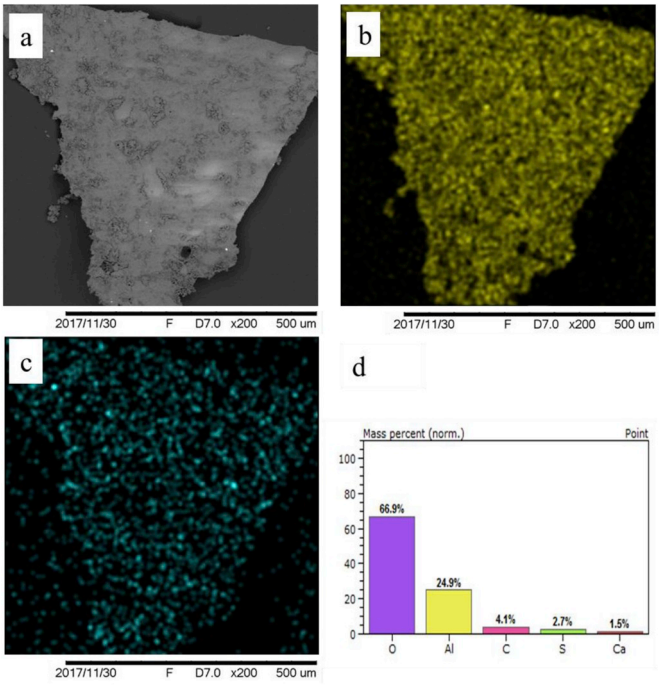

Fig. 6. (a) SEM back-scattered image of coating formed by reacting a calcite cleavage fragment in a MFR for 4 h with a feed solution containing an Al concentration of 32 mg/kg (b) Aluminum concentration map for the sample. (c) Sulfur concentration map for the sample. (d) EDS semi–quantitative mass percent of elements within the coating. All images have the same field of view. Brighter colors in the Al and S maps indicate higher concentrations. (For interpretation of the references to color in this figure legend, the reader is referred to the Web version of this article.)

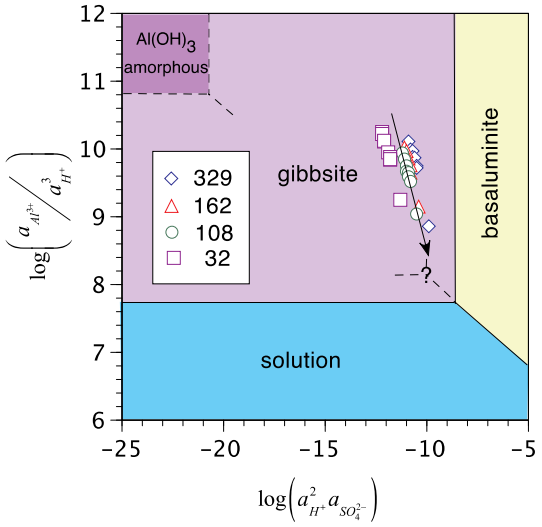

Fig. 7. Activity diagram showing the phase relationships governing the reactions that formed the coatings in the experiments. The colored symbols show how the composition of the solutions in the reactor evolved over the course of each experiment. Thermodynamic data used to construct the diagram are from Appelo and Postma (2005), Nordstrom and May (1996), Palmer and Wesolowski (1992), and Singh and Brydon (1969).

Nordstrom, 2000; Sánchez-España et al., 2011). The gibbsite stability field shown on Fig. 7 was constructed assuming coarsely crystalline gibbsite. If the gibbsite were less crystalline, the gibbsite-basaluminite-solution triple point would move toward the amorphous $Al(OH)_3$-basaluminite-solution triple point located in the upper left corner of the diagram. This track suggests that as the coatings grew, the solution composition in the reactor was evolving toward the location of protocrystalline gibbsite indicated by the "?" symbol on the diagram. This would help explain, and be consistent with, the S concentration map shown in Fig. 6c which suggests that small amounts of basaluminite may have also precipitated. An alternative explanation for the trace amounts of S in the precipitate may be sulfate sorption onto the gibbsite. Nordstrom (1982) described solid-phase solubility controls on the Al concentration in waters of high sulfate concentration and low pH. Basaluminite is generally considered to be a nanocrystalline felsöbányaite ($Al_4(OH)_{10}(SO_4)\cdot 5H_2O$) but alternatively it may be a separate mineral. There is evidence for the presence of hydrobasaluminite in streams impacted by AMD (Carrero et al., 2017; Sánchez-España et al., 2011).

The general conclusions from this study are not significantly affected if minor amounts of basaluminite formed. The amount of latent acidity released by Al precipitation is nearly the same for both phases. Gibbsite precipitation generates 3 H^+ for every Al^{3+} that is removed from the solution, as described by the equation:

$$Al^{3+} + 3\ H_2O = Al(OH)_3(gib) + 3\ H^+ \quad (4)$$

Basaluminite precipitation produces 2.5 H^+ for every Al^{3+} that is removed from the solution, as described by the equation:

$$4\ Al^{3+} + SO_4^{2-} + 15\ H_2O = Al_4(SO_4)(OH)_{10}\cdot 5H_2O(bas) + 10\ H^+ \quad (5)$$

In addition, the increase in coating thickness per mole of Al precipitated is very similar.

The fluxes of aqueous species to or from the calcite surface, as calculated using equation (3), evolved as the coatings developed. Table 1 and Fig. 8 show the Al, Ca, S, and H^+ fluxes for experiment 329–1. The positive flux for Ca indicates that Ca^{2+} produced by calcite dissolution as described by equation (1) was moving from the calcite surface to the solution. The S flux is effectively zero because sulfate does not participate in the reactions. The H^+ and Al fluxes are negative because they are consumed by reactions at the calcite and coating surfaces, respectively. Comparison of these two fluxes shows that the Al precipitation reaction, as described by equation (4), removes much more latent acidity from solution than is removed by the direct neutralization of H^+. For example, at 12960 s (see Table 1), the Al precipitation reaction consumed $(3 \times 3.53 \times 10^{-6} =)$ 106×10^{-7} mol $H^+/(m^2$ sec) from Al precipitation as compared to 3.97×10^{-7} mol $H^+/(m^2$ sec) of free acidity from solution. Thus, we observed an overall reaction that links the rates of Al precipitation and calcite dissolution, as described by the equation:

$$3\ CaCO_3 + 2\ Al^{3+} + 3\ H_2O = 3\ Ca^{2+} + Al(OH)_3 + 3\ H_2CO_3 \quad (6)$$

This reaction shows that limestone drains play a major role in removing latent acidity from AMD solutions even though the resulting coatings eventually degrade their performance. A similar equation linking limestone dissolution with Fe precipitation for a limestone drain monitoring study is shown in Cravotta and Trahan (1999).

We calculated an apparent coating thickness (x, m) using the integrated Al flux and assuming a uniform coating on all calcite surfaces. The thickness is found from the number of moles of Al deposited per

Table 1
Fluxes of dissolved species to or from the calcite surface as a function of time for experiment 329–1.

t, sec	J_{Al} mol/m²sec	J_{Ca} mol/m²sec	J_S mol/m²sec	J_{H^+} mol/m²sec
540	-2.32×10^{-5}	4.16×10^{-5}	-4.44×10^{-6}	-5.55×10^{-7}
1080	-1.84×10^{-5}	3.44×10^{-5}	-4.33×10^{-6}	-5.09×10^{-7}
1620	-1.48×10^{-5}	2.86×10^{-5}	-3.48×10^{-6}	-4.91×10^{-7}
2160	-1.21×10^{-5}	2.37×10^{-5}	-3.83×10^{-6}	-4.64×10^{-7}
3780	-6.99×10^{-6}	1.87×10^{-5}	-9.62×10^{-7}	-4.54×10^{-7}
7560	-4.06×10^{-6}	1.25×10^{-5}	-7.34×10^{-7}	-3.78×10^{-7}
12960	-3.53×10^{-6}	1.10×10^{-5}	-1.27×10^{-7}	-3.97×10^{-7}

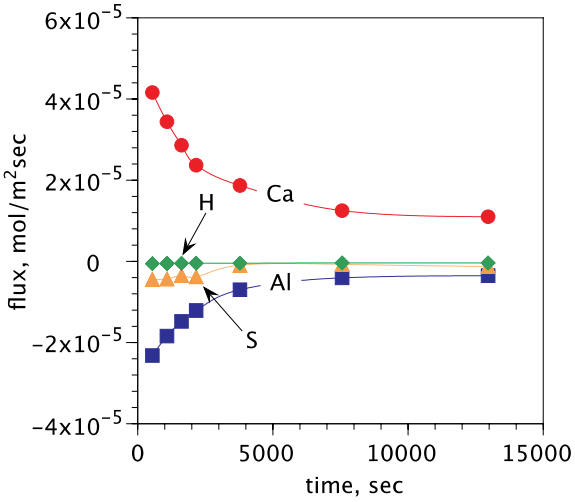

Fig. 8. Time variation of fluxes of dissolved species to (−) or from (+) the calcite surface for experiment 329–1.

square meter (n_{Al}, mol/m^2) multiplied by the molar volume of the coating (V_m, m^3/mol) and divided by (*1- ϕ*) where ϕ is the porosity, as described by the equation:

$$x = \frac{n_{Al} V_m}{1 - \phi} \tag{7}$$

In our calculations ϕ was set at 0.5. Unit cell volume data (from http://webmineral.com/) were used to calculate the molar volumes. The gibbsite unit cell contains 8 formula units and has a volume of 53.055 Å^3. This translates to a molar volume of 3.196×10^{-5} m^3. There is only 1 mol of Al in a mole of gibbsite. If the basaluminite unit cell was used it contains 24 formula units and has a volume of 8385.70 Å^3. This translates to a molar volume of 2.104×10^{-4} m^3. There are 4 mol of Al per formula unit so every mole of Al as basaluminite amounts to 5.261×10^{-5} m^3.

The number of moles of Al removed from solution per square meter of calcite surface (n_{Al}) was calculated by using the trapezoidal rule to integrate the J_{Al} data. The results for experiment 329–1 are shown in Table 2 and illustrated in Fig. 9a. The coating thickness at the end of each of the experiments is shown in Fig. 9b. The n_{Al} values were used to calculate the coating thicknesses, assuming that it was either pure gibbsite or pure basaluminite. The calculated thicknesses are on the order of a few micrometers. If the coatings were pure basaluminite they would be ~60% thicker than for pure gibbsite. However, it appears that coatings contained very little S so the effect of basaluminite formation on coating thickness appears to be inconsequential.

When the aluminum sulfate solution contacted the calcite grains reaction (1) consumed some H^+ and that caused some of the dissolved Al to hydrolyze and precipitate by reaction (4). The $Al(OH)_3$ that precipitated onto the calcite formed a coating that became a barrier to the transport of H^+ from the solution to the calcite surface. Continued gibbsite precipitation caused the observed slowing of the neutralization rate as evidenced by the declining pH of the effluent solution (Fig. 3). This implies that the diffusional flux of H^+ through the coating is a controlling factor in limestone drain performance. Fig. 10 shows a simplified model of this situation. The model assumes that the H^+ concentration at the coating surface is the same as in the bulk solution and the concentration at the calcite surface is effectively zero. Fick's first law can be used to model the flux of H^+ from the solution to the calcite surface, as described by the equation:

$$J = \frac{D}{x}\left(c_{H^+} - 0\right) \tag{8}$$

It is important to note that although the H^+ concentration at the calcite surface is low, it is not zero. Instead, it is controlled by the equilibrium constant for reaction (1) but based on this simplified model we do not know the Ca^{2+} and H_2CO_3 concentrations at the calcite surface so we cannot calculate the H^+ concentration.

Because the diffusion coefficient for Al^{3+} is very low compared to H^+, as shown in Table 3, most of the Al^{3+} hydrolysis occurred at the coating/solution interface. This reaction constantly resupplied H^+ at the coating/solution interface and replaced the H^+ lost by diffusion into the coating. That maintained a nearly constant pH at that interface. This process caused the coating to grow thicker over time, but because little or no Al^{3+} entered the coating, it did not become denser.

In order to maintain charge balance within the coating, the H^+ flux to the calcite must be balanced by two times the Ca^{2+} flux away from the calcite. This means that equation (8) can be rearranged to calculate the H^+ diffusion coefficient in the coating using the Ca^{2+} flux data, as described by the equation:

$$D_{H^+} = \frac{(2J_{Ca})x}{c_{H^+}} \tag{9}$$

Fig. 11 shows that the H^+ diffusion coefficients were nearly constant as the coatings grew thicker with time, especially in the solutions with higher starting Al concentrations. This is consistent with the idea that most of the gibbsite precipitation occurred at the coating/solution interface rather than within the coating. Furthermore, Fig. 11 shows that the H^+ diffusion coefficients in coatings that grew rapidly, from solutions with high Al^{3+} concentrations, are significantly higher than for the coatings that grew more slowly, from solutions with low Al^{3+} concentrations.

Table 2
Calculated coating thickness (*x*, m) for experiment 329–1 assuming the coating consisted of either pure gibbsite or pure basaluminite. These calculations assume that J_{Al} from 0 to 540 s was the same as the value calculated at 540 s.

t, sec	J_{Al}, mol/m^{2}sec	n_{Al}, mol	x_{bas}, m	x_{gib}, m
0	2.32×10^{-5}	0		
540	2.32×10^{-5}	0.006	1.32×10^{-6}	8.02×10^{-7}
1080	1.84×10^{-5}	0.017	2.50×10^{-6}	1.52×10^{-6}
1620	1.48×10^{-5}	0.026	3.44×10^{-6}	2.09×10^{-6}
2160	1.21×10^{-5}	0.034	4.21×10^{-6}	2.56×10^{-6}
3780	6.99×10^{-6}	0.049	5.83×10^{-6}	3.55×10^{-6}
7560	4.06×10^{-6}	0.070	8.03×10^{-6}	4.89×10^{-6}
12960	3.53×10^{-6}	0.091	1.02×10^{-5}	6.20×10^{-6}

4.1. Applications to limestone drain design

The experiment described here using aluminum sulfate solutions and calcite in a MFR provides a rapid and inexpensive way to investigate the effect of solution chemistry and coating formation for conditions likely to be found in limestone drains. The rates of change of solution concentration (*R*) for the coarser particle size found in limestone drains is found by multiplying the flux (*J*) by the ratio of limestone surface area to mass of water in the pore spaces (A/*M*), where $\frac{A}{M} = \left(\frac{(1-\phi)}{\phi}\right)\left(\frac{6}{1000D}\right)$; ϕ = porosity and *D*(m) is particle diameter, as described by the equation:

$$R\left(\frac{\text{mol}}{\text{kg sec}}\right) = \frac{A\,(\text{m}^2)}{M\,(\text{kg})} J\left(\frac{\text{mol}}{\text{m}^2\text{sec}}\right) \tag{10}$$

It is critical to evaluate both solution and solid data together in order to identify the controlling chemical reactions. Our experiment measures neutralization rates, identifies key reactions, characterizes coating mineralogy and thickness, and evaluates diffusion coefficients for H^+ in the coating. The experiment can be extended to test the effects of varying the concentration of other solution constituents. For example, adding ferric iron would cause the simultaneous precipitation of iron oxyhydroxides or increasing sulfate concentrations would cause

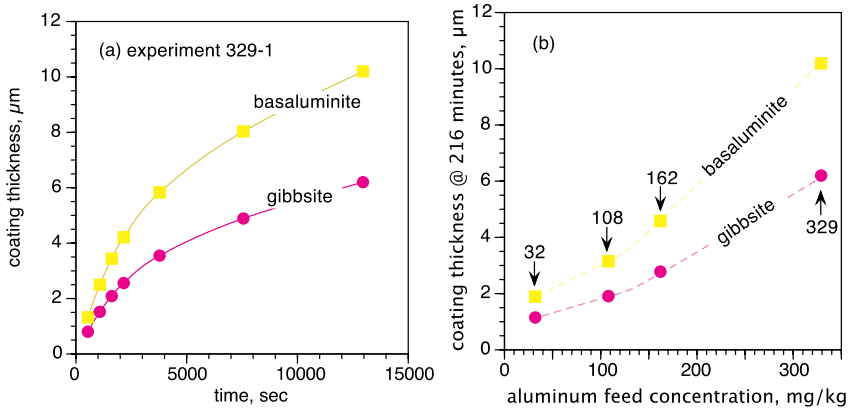

Fig. 9. (a) Coating thickness on calcite as a function of time for experiment 329–1. (b) Coating thickness on calcite at the end of experiments of 216 min duration with 32, 108, 162, and 329 mg/kg Al concentration in the feed solution.

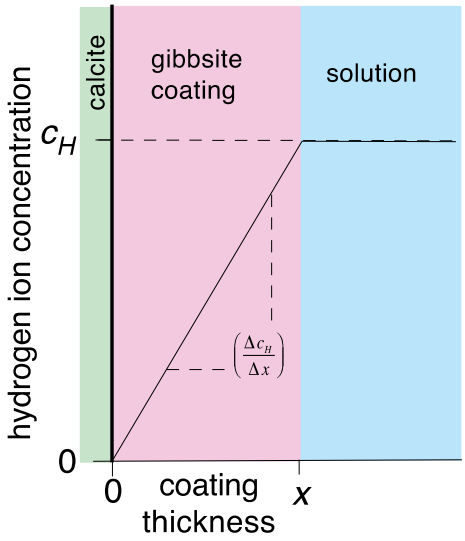

Fig. 10. Schematic illustration of the model used to calculate the diffusion coefficient for H^+ in the coatings that formed on the calcite surfaces.

Table 3
Diffusion coefficients for species involved with coating formation. The values for Ca^{2+} and H^+ are from Table 7.2 in Rimstidt (2014). The value for CO_2(aq), which is equivalent to H_2CO_3, is from Zeebe (2011). The value for Al^{3+} is based on data from van der Maarel and de Bleijser (1987) based on a polynomial fit extrapolated to zero concentration.

species	D (25 °C) m^2/sec
Al^{3+}	0.53×10^{-9}
Ca^{2+}	0.9×10^{-9}
H^+	9.3×10^{-9}
CO_2(aq)	14.7×10^{-9}

gypsum to form. The experiment can also be used to test the neutralization behavior of related substances such as dolomite (Cravotta et al., 2008; Genty et al., 2012), magnesite (Masindi et al., 2015), and steel slag (Simmons et al., 2002). It can also test the effects of possible coating modifiers, such as surfactants and biofilms, on neutralization rates. Experiments can also be designed to evaluate the effect of particle sizes and purity of limestone or possible mixtures of different materials/sizes. Collecting and analyzing this kind information are important steps toward improving the models used for limestone drain designs.

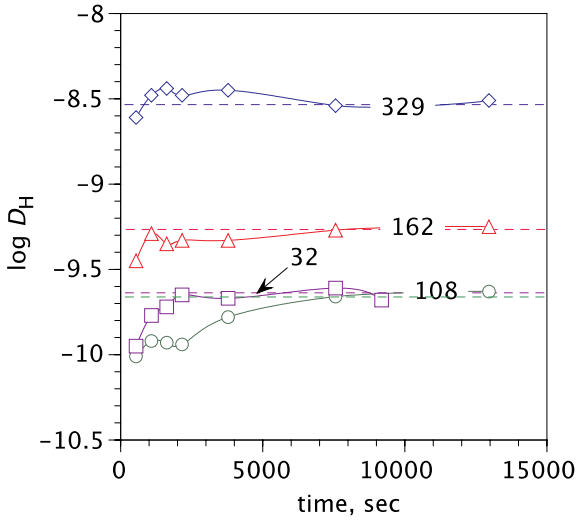

Fig. 11. Calculated H^+ diffusion coefficients (m^2/sec) in the poorly crystalline gibbsite coatings that formed in experiments 329–1, 162–1, 108–1, and 32–1 (the first number in the experiment code indicates the Al concentration in the feed solution in mg/kg). The H^+ diffusion coefficient in pure water is $10^{-8.03}$ m^2/sec (see Table 3). H^+ diffusion coefficients shown are up to two orders of magnitude slower than in pure water.

Acknowledgments

Palomino-Ore thanks the Fulbright program for the opportunity to study in the USA and the Department of Geosciences, the College of Science and the Graduate School at Virginia Tech for financial support. We thank F. Marc Michel for manufacturing the reactor used in this study. We thank Neil Johnson for help with the XRD, Qing Tang for help with the SEM, and Athena Tilley for ICP OES analyses. We greatly appreciate helpful reviews by Charles Cravotta, Kate Campbell, and Jane Hammarstrom.

Appendix A. Supplementary data

Supplementary data to this article can be found online at https://doi.org/10.1016/j.apgeochem.2019.02.004.

References

Appelo, C.A.J., Postma, D., 2005. Geochemistry, Groundwater and Pollution, second ed. CRC Press, Boca Raton, Fl.
Bigham, J., Nordstrom, D.K., 2000. Iron and aluminum hydroxysulfates from acid sulfate waters. Rev. Mineral. Geochem. 40, 351–403.
Camargo, M.M.P., Fernandes, M.N., Martinez, C.B.R., 2009. How aluminium exposure

promotes osmoregulatory disturbances in the neotropical freshwater fish *Prochilus lineatus*. Aquat. Toxicol. 94, 40–46.
Carrero, S., Fernandez-Martinez, A., Pérez-López, R., Lee, D., Aquilanti, G., Poulain, A., Lozano, A., Nieto, J.-M., 2017. The nanocrystalline structure of basaluminite, an aluminum hydroxide sulfate from acid mine drainage. Am. Mineral. 102, 2381–2389.
Cravotta III, C.A., 2003. Size and performance of anoxic limestone drains to neutralize acid mine drainage. J. Environ. Qual. 32, 1277–1289.
Cravotta III, C.A., 2008a. Dissolved metals and associated constituents in abandoned coal-mine discharges, Pennsylvania, USA. Part 1: constituent quantities and correlations. Appl. Geochem. 23, 166–202.
Cravotta III, C.A., 2008b. Laboratory and field evaluation of a flushable oxic limestone drain for treatment of net-acidic drainage from a flooded anthracite mine, Pennsylvania, USA. Appl. Geochem. 23, 3404–3422.
Cravotta III, C.A., Brightbill, R.A., Langland, M.J., 2010. Abandoned mine drainage in the Swatara Creek Basin, Southern Anthracite Coalfield, Pennsylvania, USA: 1. Stream water quality trends coinciding with the return of fish. Mine Water Environ. 29, 176–199.
Cravotta III, C.A., Trahan, M.K., 1999. Limestone drains to increase pH and remove dissolved metals from acidic mine drainage. Appl. Geochem. 14, 581–606.
Cravotta III, C.A., Ward, S.J., Hammarstrom, J.M., 2008. Downflow limestone beds for treatment of net-acidic, oxic, iron-laden drainage from a flooded anthracite mine, Pennsylvania, USA: 2. Laboratory evaluation. Mine Water Environment 27, 86–99.
Cravotta III, C.A., Ward, S.J., Koury, D.J., Koch, R.D., 2004. Optimization of limestone drains for long-term treatment of mine drainage, Swatara Creek Basin, Schuylkill County, PA. In: 2004 National Meeting of the American Society of Mining and Reclamation. ASMR, Lexington, KY, pp. 366–411.
Cravotta III, C.A., Watzlaf, G.R., 2002. Design and performance of limestone drains to increase pH and remove metals from acidic mine drainage, Handbook of Groundwater Remediation Using Permeable Reactive Barriers. Elsevier, pp. 19–66.
Gensemer, R.W., Playle, R.C., 1999. The bioavailability and toxicity of aluminum in aquatic environments. Crit. Rev. Environ. Sci. Technol. 29, 315–450.
Genty, T., Bussirére, B., Potvin, R., Benzaazoua, M., Zagury, G.J., 2012. Dissolution of calcitic marble and dolomitic rock in high iron concentrated acid mine drainage: application to anoxic limestone drains. Environ. Earth Sci. 66, 2387–2401.
Hammarstrom, J.M., Sibrell, P.L., Belkin, H.E., 2003. Characterization of limestone reacted with acid-mine drainage in a pulsed limestone bed treatment system at the Friendship Hill National Historical Site, Pennsylvania, USA. Appl. Geochem. 18, 1705–1721.
Hedin, R.S., Watzlaf, G.R., Nairn, R.W., 1994. Passive treatment of acid mine drainage with limestone. J. Environ. Qual. 23, 1338–1345.
Henry, T.B., Irwin, E.R., Grizzle, J.M., Wildhaber, M.L., Brumbaugh, W.G., 1999. Acute toxicity of an acid mine drainage mixing zone to Juvenile Bluegill and Largemouth bass. Trans. Am. Fish. Soc. 128, 919–928.
Huminicki, D.M.C., Rimstidt, J.D., 2008. Neutralization of sulfuric acid solutions by calcite dissolution and the application to anoxic limestone drain design. Appl. Geochem. 23, 148–165.
Huminicki, D.M.C., Rimstidt, J.D., 2009. Iron oxyhydroxide coating of pyrite for acid mine drainage control. Appl. Geochem. 24, 1626–1634.
Kirby, C.S., Cravotta, C.A., 2005. Net alkalinity and net acidity 2: practical considerations. Appl. Geochem. 20, 1941–1964.
Masindi, V., Gitari, M.W., Tutu, H., DeBeer, M., 2015. Passive remediation of acid mine drainage using cryptocrystalline magnesite: a batch experimental and geochemical modelling approach. Water SA 41, 677–682.
Michel, F.M., Rimstidt, J.D., Kletetschka, K., 2018. 3D printed mixed flow reactor for geochemical rate measurements. Appl. Geochem. 89, 86–91.
Nordstrom, D.K., 1982. The effect of sulfate on aluminum concentrations in natural waters: some stability relations in the system Al_2O_3-SO_3-H_2O at 298 K. Geochim. Cosmochim. Acta 46, 681–692.
Nordstrom, D.K., May, H.M., 1996. Aqueous equilibrium data for mononuclear aluminum species. In: Sposito, G. (Ed.), The Environmental Chemistry of Aluminum. CRC Press, Boca Raton, Florida, pp. 39–80.
Palmer, D.A., Wesolowski, D.J., 1992. Aluminum speciation and equilibria in aqueous - solution. 2. The solubility of gibbsite in acidic sodium - chloride solutions from 30-degrees-C to 70-degrees-C. Geochim. Cosmochim. Acta 56, 1093–1111.
Plumlee, G.S., Smith, K., Montour, M., Ficklin, W., Mosier, E., 1999. Geologic controls on the composition of natural waters and mine waters draining diverse mineral-deposit types. Rev. Econ. Geol. 6B, 373–432.
Rimstidt, J.D., 2014. Geochemical Rate Models. Cambridge University Press, Cambridge.
Rimstidt, J.D., 2015. Diffusion control of quartz and forsterite dissolution rates. Appl. Geochem. 61, 99–108.
Rimstidt, J.D., Dove, P.M., 1986. Mineral/solution reaction rates in a mixed flow reactor: Wollastonite hydrolysis. Geochim. Cosmochim. Acta 50, 2509–2516.
Robbins, E., Cravotta III, C., Savela, C., Nord Jr., G., 1999. Hydrobiogeochemical interactions in anoxic limestone drains for neutralization of acidic mine drainage. Fuel 78, 259–270.
Sánchez-España, J., Yusta, I., Diez-Ercilla, M., 2011. Schwertmannite and hydrobasaluminite: a re-evaluation of their solubility and control on the iron and aluminium concentration in acidic pit lakes. Appl. Geochem. 26, 1752–1774.
Santomartino, S., Webb, J.A., 2007. Estimating the longevity of limestone drains in treating acid mine drainage containing high concentrations of iron. Appl. Geochem. 22, 2344–2361.
Santoro, L., Volpicelli, G., Caprio, V., 1987. Limestone neutralization of acid waters in the presence of surface precipitates. Water Res. 21, 641–647.
Simmons, J., Ziemkiewicz, P., Black, D.C., 2002. Use of steel slag leach beds for the treatment of acid mine drainage. Mine Water Environ. 21, 91–99.
Singh, S.S., Brydon, J.E., 1969. Solubility of basic aluminum sulfates at equilibrium in solution and in the presence of montmorillonite. Soil Sci. 107, 12–16.
Skousen, J., Ziemkiewicz, P., 2005. Performance of 116 passive treatment systems for acid mine drainage. In: 2005 National Meeting for the American Society of Mining and Reclamation. ASMR, Breckenridge, CO.
Skousen, J., Zipper, C.E., Rose, A., Ziemkiewicz, P.F., Nairn, R., McDonald, L.M., Kleinmann, R.L., 2017. Review of passive systems for acid mine drainage treatment. Mine Water Environ. 36, 133–153.
Soucek, D.J., Cherry, D.S., Zipper, C.E., 2003. Impacts of mine drainage and other non-point source pollutants on aquatic biota in the Upper Powell River system, Virginia. Hum. Ecol. Risk Assess. Int. J. 9, 1059–1073.
Teien, H.-C., Kroglund, F., Salbu, B., Rosseland, B.O., 2006. Gill reactivity of aluminium-species following liming. Sci. Total Environ. 358, 206–220.
van der Maarel, J.R.C., de Bleijser, J., 1987. Water and aluminum self-diffusion in aqueous $AlCl_3$ solutions. Chem. Phys. Lett. 141, 251–254.
Volpicelli, G., Caprio, V., Santoro, L., Ciambelli, P., 1981. Neutralization of acid waters containing aluminum ions by means of limestone. Chem. Eng. J. 21, 29–38.
Watzlaf, G.R., Schroeder, K.T., Kairies, C.L., 2000. Long-term performance of anoxic limestone drains. Mine Water Environ. 19, 98–110.
Zeebe, R.E., 2011. On the molecular diffusion coefficients of dissolved CO_2, HCO_3^-, and CO_3^{2-} and their dependence on isotopic mass. Geochim. Cosmochim. Acta 75, 2483–2498.